PAPER • **OPEN ACCESS**

Numerical Investigation on the Temperature dependent Impedance Characteristics of Far-Infrared Quantum Cascade Lasers

To cite this article: P Ashok *et al* 2023 *J. Phys.: Conf. Ser.* **2466** 012018

Numerical Investigation on the Temperature dependent Impedance Characteristics of Far-Infrared Quantum Cascade Lasers

P Ashok*[1], M Ganesh Madhan[2], S Gopinath[3], T R Premila[4], N Janaki[5]

[1]Associate Professor, Symbiosis Institute of Digital and Telecom Management (SIDTM), Symbiosis International (Deemed University) (SIU), Pune, Maharashtra, India.

[2]Professor, Madras Institute of Technology, Anna University, Chennai, Tamilnadu, India.

[3]Professor, Karpagam Institute of Technology, Coimbatore, Tamilnadu, India.

[4,5]Assistant Professor, Vels Institute of Science Technology and Advanced Studies, Chennai, Tamilnadu, India.

*Corresponding author's e-mail: p.ashok@sidtm.edu.in

Abstract. Quantum Cascade Lasers (QCLs) as Terahertz (THz) frequency sources offer a potentially viable solution for new applications in mid and far-infrared frequency bands. This research work exhaustively investigates the temperature dependence on the impedance of temperature dependent Quantum Cascade Lasers (QCLs) operating at 116μm, for the first time. In the 90-stage QCL considered for the work, the cold finger temperature is varied from 15K to 45K. When the device is biased at 0.6A current along with a cold finger temperature of 45K, the magnitude of intrinsic impedance was found to be 23.91mΩ, at a frequency of 4GHz. As the cold finger temperature is increased from 15K to 45K, the impedance response of the device becomes flat and stays constant. At 45K with an injected current of 1.5A, maximum impedance of 3.1mΩ is obtained. The resonant frequency characteristics of the device increase with increase in injected current and cold finger temperature. Also, it is observed that the magnitude of intrinsic impedance decreases with increase in injected current. The impact of cold finger temperature on the intrinsic impedance characteristics are detailed for prospective Radio over Fiber (RoF) applications.

1. Introduction

QCLs are one of the most promising sources of high-power terahertz radiation generated by inter sub-band transition [1]. Very recently, QCLs operate at room temperature produce larger power [2, 3]. The mid-IR region of operation of QCLs aids in detection of gaseous molecules in the atmosphere [4]. Gain switching based applications of QCL are well documented in [5-7]. Free Spaced Optics based applications of QCL are simulated and analyzed in [8-12]. Impedance characteristics have been well documented for QCLs and semiconductor laser diodes [8, 13]. Bistable behavior has been theoretically analyzed in normal and Quantum cascade lasers [11, 14]. The design of an end-to-end QCL based FSO link incorporating the device parameters is analyzed in [15]. However, an exhaustive numerical simulation on the temperature dependence of impedance for this device has not been documented anywhere. Hence, this work numerically computes the intrinsic impedance of the device for various cold finger temperatures and at different currents. The impedance characteristics of the device is vital for developing electrical signal sources to drive the QCL efficiently. The device considered for the study has threshold currents of 0.44A, 0.49A and 0.54A at cold finger temperatures of 15K, 35K and 45K respectively [16, 17]. The rate equations of temperature dependent QCL are solved numerically, to evaluate the device characteristics.

2. Computation of Intrinsic Impedance from rate equations

Temperature dependent QCLs are modelled using three-level rate equations [16, 17] as given from equation 1 to 5 below.

$$\frac{dS(t)}{dt} = \frac{-S(t)}{\tau_p} + \frac{\beta_{sp}}{\tau_{sp}(T,V)} N_3(t) + MG(T,V)\frac{\left(N_3(t) - N_2(t)\right)}{1 + \epsilon S(t)} S(t) \quad (1)$$

$$\frac{dN_3(t)}{dt} = -G(T,V)\frac{\left(N_3(t) - N_2(t)\right)}{1 + \epsilon S(t)} S(t) - \frac{1}{\tau_3(T,V)} N_3(t) + \frac{\eta_3(T,V)}{q} I(t) \quad (2)$$

$$\frac{dN_2(t)}{dt} = G(T,V)\frac{\left(N_3(t) - N_2(t)\right)}{1 + \epsilon S(t)} S(t) + \frac{1}{\tau_{32}(T,V)} N_3(t) + \frac{\eta_2(T,V)}{q} I(t) - \frac{1}{\tau_{21}(T,V)} N_2(t) \quad (3)$$

$$\frac{dT(t)}{dt} = \frac{1}{mc_p}\left(I(t)V\big(T(t), I(t)\big) - \frac{(T(t) - T_0)}{R_{th}}\right) \quad (4)$$

$$P_{opt} = \eta_0 \hbar\omega S(t)/\tau_p \quad (5)$$

Where N_3, N_2, S, P_{opt} denote electron numbers in level 3 and 2, photon number and optical power output from the QCL respectively. T and V represent cold finger temperature and junction voltage respectively. Upon solving the rate equations, steady state characteristics are obtained and figure 1 represents the steady state characteristics of the device having a threshold current of 0.44A, 0.49A and 0.54A at 15K, 35K and 45K respectively, under voltage independent and dependent conditions. The steady state temperature of the device is shown in figure 1c. Since the steady state results are exactly identical with the results of [16, 17], small signal analysis is done now to formulate the impedance of the device. All the variables exhibit complex exponential variation as denoted from equation 6 to 11.

$$N_3 = N_{3s} + N_3(\omega)\, e^{j\omega t} \quad (6)$$

$$N_2 = N_{2s} + N_2(\omega) e^{j\omega t} \quad (7)$$

$$S = S_s + S(\omega)\, e^{j\omega t} \quad (8)$$

$$T = T_s + T(\omega)\, e^{j\omega t} \quad (9)$$

$$I = I_s + I(\omega)\, e^{j\omega t} \quad (10)$$

$$V = V_s + V(\omega)\, e^{j\omega t} \quad (11)$$

In the above equations, the variables suffixed with 's' indicate their steady state values. Upon solving, equation 1 to 4 and equation 6 to 11 by substitution and re-arranging, the values of $N_3(\omega)$, $N_2(\omega)$, $S(\omega)$ are deduced. The calculations are shown below.

$$N_3(\omega) = \frac{\frac{\eta_3\, I(\omega)}{q} - G(N_{3s} - N_{2s})S(\omega) + GN_2(\omega)S_s}{j\omega + \frac{1}{\tau_3} + GS_s} \quad (12)$$

$$N_2(\omega) = \frac{\frac{\eta_2\, I(\omega)}{q} + N_3(\omega)\left(GS_s - \frac{1}{\tau_{32}}\right) + G(N_{3s} - N_{2s})S(\omega)}{j\omega + \frac{1}{\tau_{21}} + GS_s} \quad (13)$$

$$S(\omega) = \frac{N_3(\omega)(MGS_s + \frac{\beta}{\tau_{sp}}) - MGS_sN_2(\omega)}{j\omega + \frac{1}{\tau_p} - MG(N_{3s} - N_{2s})} \quad (14)$$

$$T(\omega) = \frac{T_0 + VI(\omega)R_{th}}{1 + j\omega mc_p R_{th}} \tag{15}$$

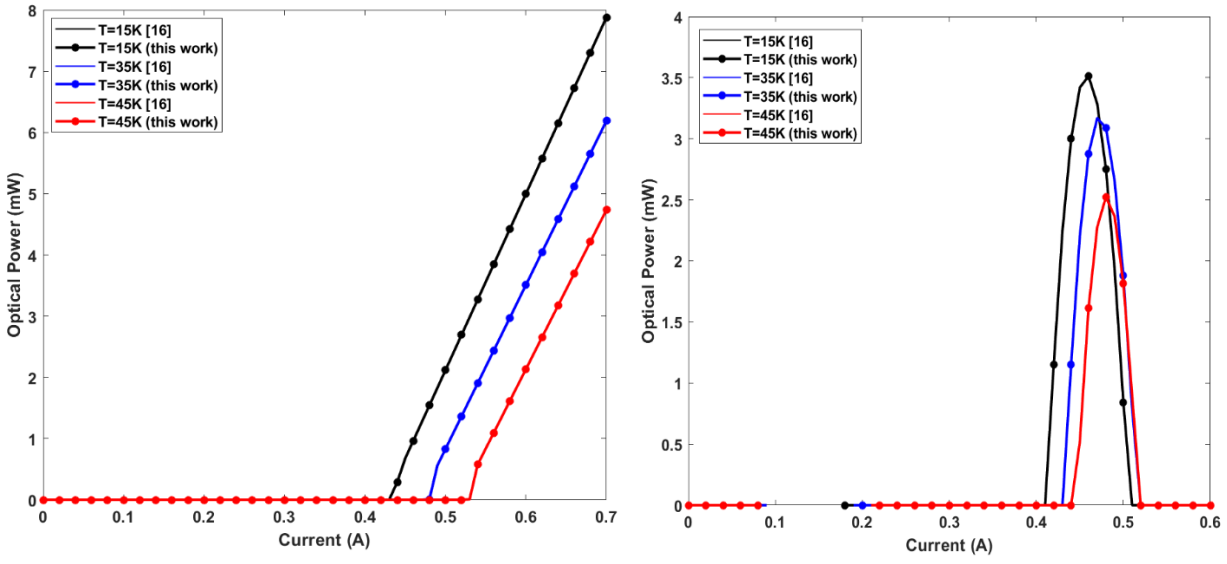

(a) (b)

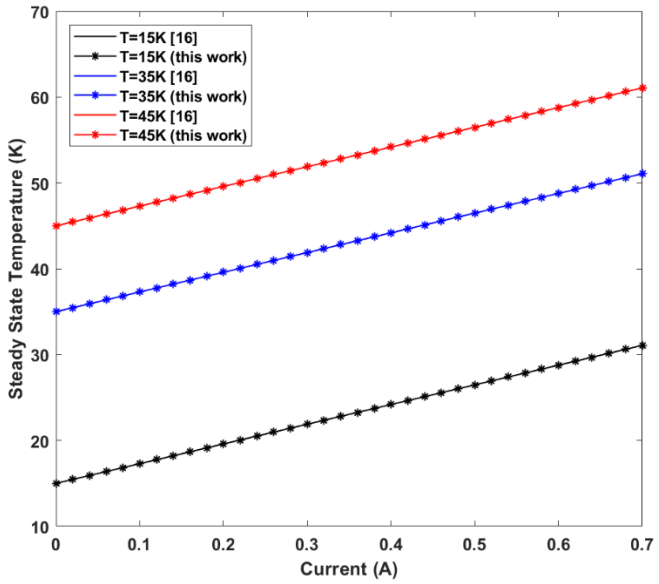

(c)

Figure 1 (a) Voltage independent Current-Power characteristics of QCL (b) Voltage dependent Current-Power characteristics of QCL (c) Voltage independent Current-Temperature characteristics of QCL

Equations 12, 13, 14 and 15 give the frequency dependent expression for all the variables involved. Eq. 21 characterizes the impedance of the device under varying frequency and currents, where V_T (=kT/q) signifies the thermal equivalent voltage.

$$N_3 = N_{3i}\, e^{\frac{qV_3}{2kT}} \tag{16}$$

$$N_2 = N_{2i}\, e^{\frac{qV_2}{2kT}} \tag{17}$$

$$V_3(\omega) = \frac{N_3(\omega)}{N_{3s}} * 2V_T \tag{18}$$

$$V_2(\omega) = \frac{N_2(\omega)}{N_{2s}} * 2V_T \tag{19}$$

$$V(\omega) = V_3(\omega) - V_2(\omega) = 2V_T\left(\frac{N_3(\omega)}{N_{3s}} - \frac{N_2(\omega)}{N_{2s}}\right) \tag{20}$$

$$Z(\omega) = \frac{V(\omega)}{I(\omega)} \tag{21}$$

The frequency dependent impedance characteristics of QCL as obtained by computing Z(ω) using equation 21 is shown in figure 2.

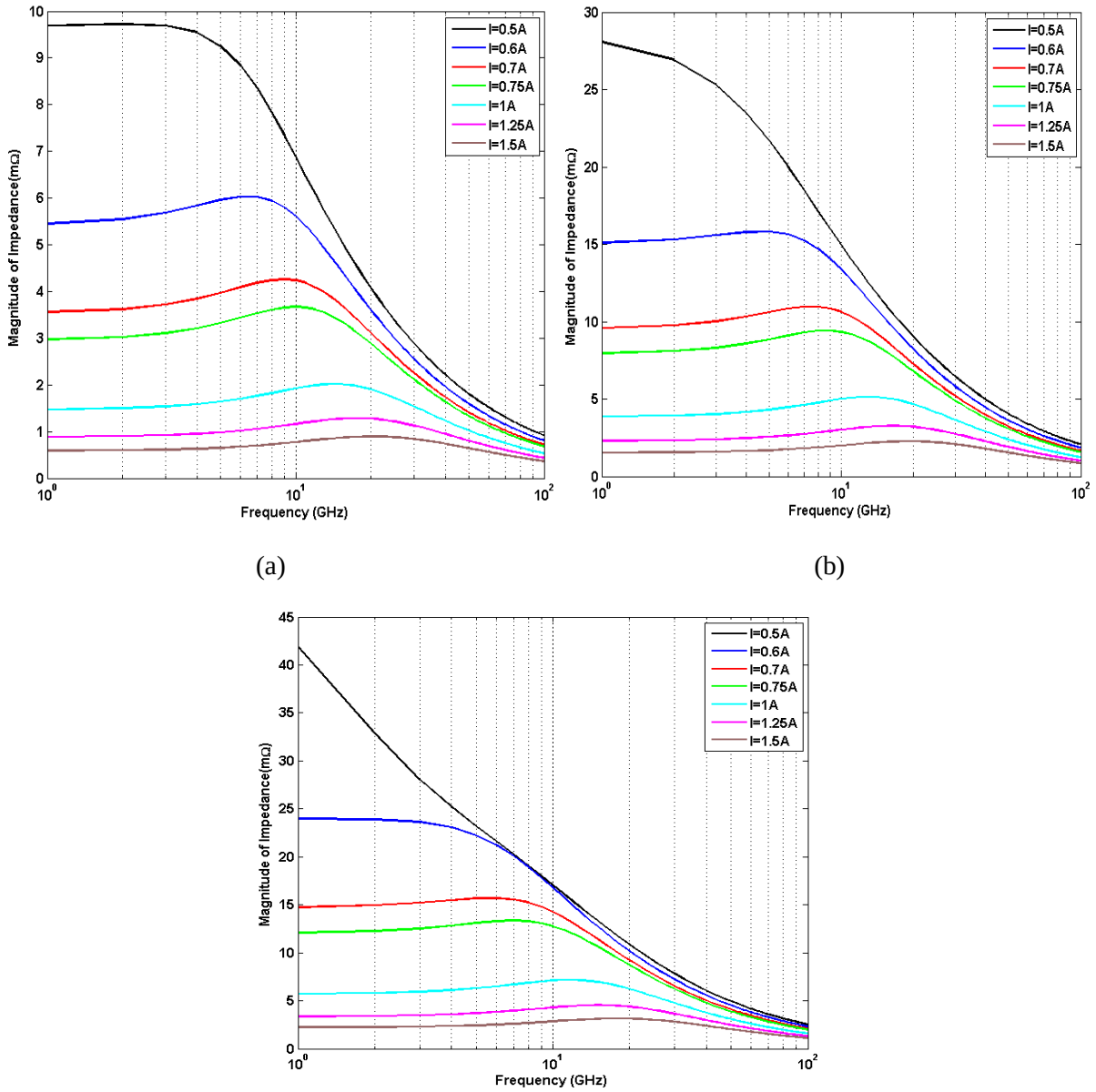

Figure 2 Impedance Characteristics of the device for (a) T=15K (b) T=35K (c) T=45K

Resonance is exhibited by this device at a particular frequency for a given current. Since the device is lasing at a particular wavelength, resonance also occurs around this wavelength. The resonant frequency slightly shifts towards the higher side due to change in injected current or operating

conditions of the device. The resonance effect is more pronounced at a cold finger temperature of 15K.The same is observed in figure 2. When the injected current is close to threshold current at a particular cold finger temperature, the impedance characteristics remain flat and fall off as the frequency is increased. At higher currents, resonance is exhibited. This behavior is depicted clearly in figure 2 for various cold finger temperatures of 15K, 35K and 45K. Until resonance, the impedance remains constant. The intrinsic impedance and the resonant frequency are found for various injected currents and at different cold finger temperatures. The result is shown in figure 3.

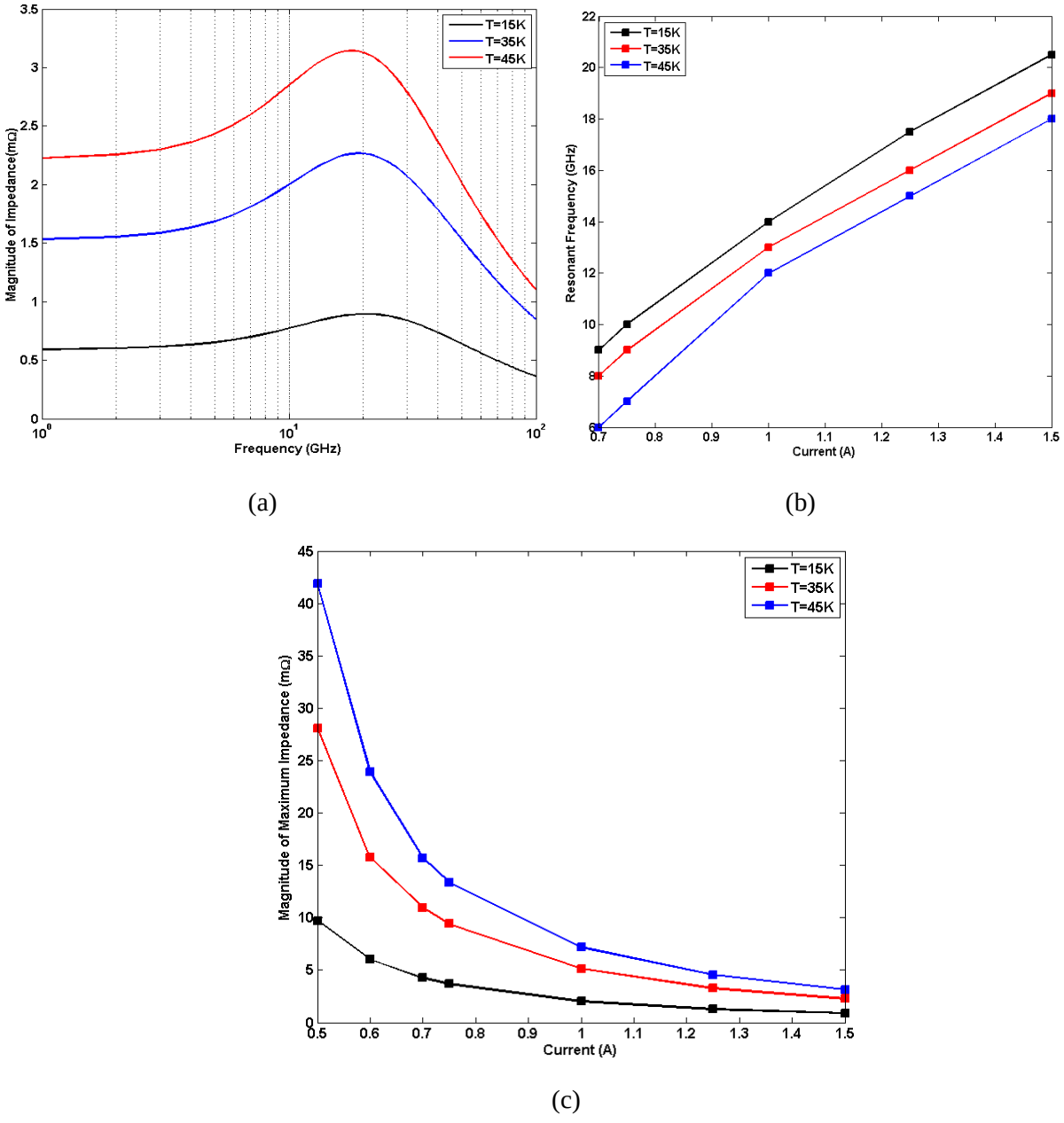

(a) (b)

(c)

Figure 3 (a) Impedance Characteristics at 1.5A for various cold finger temperatures (b) Current vs Resonant Frequency characteristics (c) Current vs Impedance characteristics

From figure 3a, it is evident that at 1.5A of current injected into the device, the magnitude of impedance is maximum at 45K while it is least at 15K. This behavior is observed for all currents. As the injected current is increased, the resonant frequency also increases linearly. For any given current, resonant frequency is always maximum at 15K as in figure 3b. Further, impedance decreases as the magnitude of injected current is increased as depicted in figure 3c.

3. Conclusion

In this work, computation of temperature dependent intrinsic impedance of QCL is reported for the first time. Simulation results conclude that, for a cold finger temperature of 45K and injected current of 0.6A, the intrinsic impedance was found to be 23.91mΩ at a frequency of 4GHz. As the cold finger temperature is increased from 15K to 45K, the impedance response of the device becomes flat and stays constant. This constant impedance characteristics of the device can be exploited for potential RoF and 5G applications. Irrespective of the current injected into the device, the magnitude of intrinsic impedance is always maximum at 45K. At 45K with an injected current of 1.5A, maximum impedance of 3.1mΩ is obtained. The resonant frequency characteristics of the device increase with increase in injected current and cold finger temperature. Also, it is observed that the magnitude of intrinsic impedance decreases with increase in injected current.

References

[1] Razeghi M 2009 IEEE *J. Sel. Top. Quantum Electron.,* **15(3)** 941–951.
[2] Bai Y, Bandyopadhyay N, Tsao S, Slivken S and Razeghi M 2011 *Appl. Phys. Lett.* **98(18)** 181102.
[3] Bai Y, Slivken S, Kuboya S, Darvish S R and Razeghi M 2010 *Nat. Photonics* **4(2)** 99–102.
[4] Bandyopadhyay N, Bai Y, Tsao S, Nida S, Slivken S and Razeghi M 2012 *Appl. Phys. Lett.* **101(24)** 241110.
[5] Ashok P and Ganesh Madhan M 2019 *Laser Phys. Lett.* **16(9)**, 1–6.
[6] Ashok P and Ganesh Madhan M 2020 *Laser Phys. Lett.* **17(5)** 1–7.
[7] Murali Krishna K, Ganesh Madhan M and Ashok P 2020 *Def. Sci. J*, **70(5)**, 538-541.
[8] Ashok P and Ganesh Madhan M 2021 *J. Opt. Laser Technol.* **134**, 106662.
[9] Gopinath S, Ashok P and Ganesh Madhan M 2021 *Laser Phys. Lett.,* **18(6)**, 1-5.
[10] Murali Krishna K, Ganesh Madhan M and Ashok P 2022 *Optik* **257** 168740, 1-11.
[11] Ashok P and Ganesh Madhan M 2020 *Optik* **204** 164216.
[12] Murali Krishna K, Ganesh Madhan M and Ashok P 2020 *Optik* **219** 165018.
[13] Ozyazici M S 2004 *J. Optoelectron. Adv. Mater.*, **6(4)** 1243 – 1253.
[14] Ganesh Madhan M, Gunasekaran N, Pukhraj Vaya (1998) *Int J Optoelectron* **12(3)** 99-104.
[15] Ashok P, Ganesh Madhan M and Natraj N A 2021 *Laser Phys. Lett.* **18(3)** 1-6.
[16] Agnew G 2017 *IEEE J. Sel.Top. Quantum Electron.* **23** 1–9.
[17] Agnew G 2015 *Appl.Phys. Lett.* **106** 161105.
[18] Weisser S, Esquivias I, Tasker P J, Ralston J D, Romero B and Rosenzweig J 1994 *IEEE Photonic Tech L* **6(12)** 1421-1423.